JCTC Journal of Chemical Theory and Computation

Parametrization and Validation of Coarse Grained Force-Fields Derived from ab Initio Calculations

Giacomo Prampolini*

Dipartimento di Chimica e Chimica Industriale, Università di Pisa, via Risorgimento 35, I-56126 Pisa, Italy

Received December 23, 2005

Abstract: A novel multisite interaction potential, suitable for computer simulations of complex materials as liquid crystals or polymers, is proposed and parametrized. Its validation is achieved through Monte Carlo numerical experiments at constant temperature and pressure, performed on the *p*-*n*-phenyls series and a typical mesogenic molecule (5CB). The model is constructed by connecting an array of anisotropic Gay-Berne sites and a collection of isotropic Lennard-Jones sites. The former mimics the rigid planar six-membered rings of the molecule, while the latter represents the flexible chain, if present. Such intermolecular potential, coupled with an intramolecular part to account for molecular flexibility, is parametrized from ab initio information only, obtained through the recently proposed Fragmentation-Reconstruction Method (FRM). Computer simulations are performed on all systems by exploring phase behavior at several temperatures and by comparing the resulting thermodynamic and structural properties with the relevant experimental data. Despite the simplicity of the present models, the good agreement with the experimental measures suggests the possibility of adopting such hybrid potentials for those systems with a large number of atoms, where high computational cost does not allow the use of more accurate atomistic potentials.

1. Introduction

In the past decades, computer simulations have considerably aided the study of advanced materials such as liquid crystals or polymers.[1,2] Unlike simple liquids, both the wide range of length and time scales that characterizes the dynamics of such complex substances, and the large dimensions of their forming molecules have suggested the adoption of simplified or coarse grained models.[2−5] In liquid crystal field, for instance, many anisotropic single site interaction models have been reported in the literature.[6−9] Among them, the most successfully employed is certainly the Gay-Berne (GB) potential,[3,9−11] which has much contributed to clarify the basic features responsible for mesogenic behavior. The main lack of these single-site models is the absence of molecular flexibility, which cannot be neglected if one aims to accurately reproduce experimental behavior. On the other hand, the use of atomistic force-fields becomes rapidly unfeasible with the growth of the molecular dimensions. Even standard united atom (UA) approaches, by which groups of methyl and methylene atoms are represented with a single Lennard-Jones (LJ) interaction site, might not solve the problem if one aims to sensibly increase the speed of the calculation or the quality of the statistics.

For these reasons, several models have been proposed in the past few years,[1,2,12−20] where a reasonable computational cost is reached through a reduction of the number of interaction sites, without losing the basic features of the molecular interactions. For instance, following the UA approach, LaPenna and co-workers[13] have first employed a coarse grained model potential, by coupling one GB anisotropic potential (representing the rigid molecular core of a typical mesogenic substance) with a collection of standard LJ sites describing the flexible aliphatic chain. Such a hybrid GB/LJ model has then been refined and successfully adopted in simulations of both polymers[21,22] and liquid crystals.[14,15,17,20] Despite their simplicity, in fact, hybrid models

* Corresponding author e-mail: giacomo@dcci.unipi.it.

10.1021/ct050328o CCC: $33.50
Published on Web 03/28/2006

have proven valuable to study the basic structure−property relationships subtending the bulk behavior. Nevertheless, it should be mentioned that most of these force-fields[13−15,21,22] were parametrized in a semiempirical manner, being their aim to represent the features of a general (liquid−crystalline or polymeric) bulk phase, rather than reproduce with good accuracy the experimental properties of a specific substance. Even in the most recent works,[17,20] the proposed hybrid GB/LJ model is parametrized on an empirical potential derived from the widely used OPLS[23] atomistic force-field. This route of parametrization might be inappropriate when the interest focuses on a specific substance, with a well defined molecular composition. To reproduce the thermodynamic, structural, and dynamic properties of a real advanced material, one needs to employ model potential functions able to accurately describe the interactions between its forming molecules, taking into account the chemical details that characterize the microscopic structure.

The Fragmentation Reconstruction Method (FRM), recently proposed by our group,[18,19,24−26] allows to compute, through accurate ab initio calculations, the interaction potential energy surface (PES) of dimers of large molecular dimensions. Once the FRM-PES has been computed, it can be used to parametrize the intermolecular potential model through a fitting procedure, at several possible degrees of accuracy and complexity. In this work, a model potential based on representing the phenyl groups in each molecule with single interaction sites is parametrized on the base of previously computed FRM data[18,19,24,25] and employed in MC computer simulations.

Two test cases have been chosen to validate the aforementioned model and its parametrization procedure: the *p*-*n*-phenyls series ($n = 2-5$) and 4-*n*-pentyl 4′-cyanobiphenyl (5CB), a typical mesogenic molecule. The series of *p*-polyphenyls certainly exhibits fascinating properties both in the field of polymers and liquid crystals. In the former, the applications of poly(*p*-phenylene) vary from ribbons and fibers to solid-state lubricants, and the polymer itself has been the object of several reviews.[27] In the latter, *p*-quinquephenyl and *p*-sexiphenyl show nematic and smectic phases, respectively. Moreover, the torsional potential between the phenyl rings of all the series has been recently modeled by our group[28] through accurate DFT calculations. The coupling of such an intramolecular term to the intermolecular hybrid potential should refine the results of preliminary runs already reported for these systems.[19] On the other hand, the 5CB molecule has been the object of several simulation studies,[12,16,17,20,26,29−34] being a sort of prototype nematogen. Empirical atomistic simulation models[26,30−34] have been proven capable to reproduce with a certain accuracy most of the static and dynamic properties of such liquid−crystal nematic phase. Moreover, an atomistic force-field, derived by our group through the FRM approach,[25] has been successfully employed to reproduce the bulk behavior of crystalline, nematic, and isotropic 5CB, yielding a phase diagram in good agreement with the experimental trends. However, since atomistic modeling cannot be extended to much larger molecules, a hybrid potential parametrization of 5CB PES is tempted in this work and compared with the results achieved by the atomistic model, so to evaluate the possibility of its use for computationally more expensive systems.

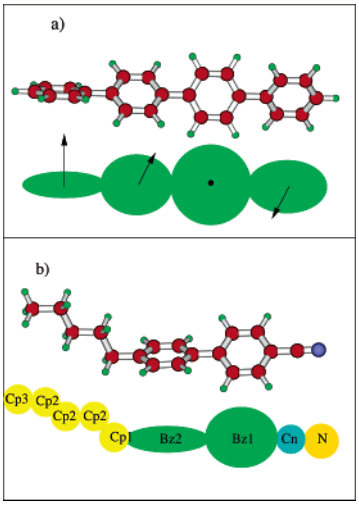

Figure 1. (a) The adopted model is shown for *p*-quaterphenyl. All the series members have been modeled in analogous manner. The black arrows on each disk represent the added quadrupoles. (b) The hybrid GB/LJ modeling is reported for 5CB. All UA interaction sites have been represented with a LJ potential, except the phenyl rings, which have been modeled with a generalized GB potential (green disks). For both models, all parameters are listed in Tables 1−2 and 4, respectively.

The paper is organized as follows. Section 2 gives details on the hybrid potential and on the employed MC technique. In the first part of section 3, the results of the parametrization of both *p*-*n*-phenyls and 5CB are discussed. In the second part, the simulation results are reported and compared with the relevant experimental data. A comparison with the results of the more detailed atomistic model[25] is also discussed. Finally, section 4 collects the main conclusions.

2. Computational Details

2.1. Hybrid Force-Fields and Fitting Procedure. *p*-Polyphenyls. All the considered *p*-*n*-phenyls ($n = 2-5$) have been modeled by representing the phenyl rings of each molecule with oblate Gay-Berne ellipsoids,[9,10] plus a linear quadrupole (Q) along the orientational axis of the disk (i.e. perpendicular to the phenyl plane). The upper panel of Figure 1 shows the adopted model for the third member of the series, namely *p*-quaterphenyl. The word "hybrid" here stands to indicate the use, in modeling one molecule, of several bonded GB sites, normally used as a single site potential.[3]

In this hybrid model, the intermolecular potential U_{AB}^{inter} between two interacting sites A and B is thus expressed by a sum of two terms, i.e.

$$U_{AB}^{inter} = U_{AB}^{gGB} + U_{AB}^{Q} \quad (1)$$

With regards to the first term of eq 1, a pair of nonequivalent GB interaction sites can be defined[9,10,19] by the specification of two parameter arrays, namely $\mathbf{P}_k = [\sigma_k^0,\sigma_k^{ee},\sigma_k^{ss},\epsilon_k^0,\epsilon_k^{ee},\epsilon_k^{ss},\mu_k,\nu_k,\xi_k]$, with $k = A, B$.

Their interaction energy, the generalized Gay-Berne potential (U_{AB}^{gGB}),[10] depends on the distance vector $\hat{r}_{AB}$ and on the disks orientational axes $\hat{u}_A$ and $\hat{u}_B$

$$U_{AB}^{gGB} = E_{AB} \times [(S_{AB})^{12} - (S_{AB})^{6}] \tag{2}$$

where

$$S_{AB} = \frac{\sigma_{AB}^{0}\xi_{AB}}{r_{AB} - \sigma_{AB}(\hat{u}_A, \hat{u}_B, \hat{r}_{AB}) + \sigma_{AB}^{0}\xi_{AB}} \tag{3}$$

and

$$E_{AB} = 4\epsilon_{AB}^{0}[\epsilon_{AB}^{(1)}(\hat{u}_A, \hat{u}_B)]^{\nu_{AB}}[\epsilon_{AB}^{(2)}(\hat{u}_A, \hat{u}_B, \hat{r}_{AB})]^{\mu_{AB}} \tag{4}$$

In eqs 3 and 4, the functions $\sigma_{AB}(\hat{u}_A, \hat{u}_B, \hat{r}_{AB})$, $\epsilon_{AB}^{(1)}(\hat{u}_A, \hat{u}_B)$, and $\epsilon_{AB}^{(2)}(\hat{u}_A, \hat{u}_B, \hat{r}_{AB})$ are defined in terms of the quantities χ_{AB}, α_{AB}, χ'_{AB}, and α'_{AB} through eqs 5−7, i.e.

$$\sigma_{AB}(\hat{u}_A, \hat{u}_B, \hat{r}_{AB}) = \sigma^{0}_{AB}\left[1 - \chi_{AB}\frac{(\alpha_{AB}^{2}(\hat{r}_{AB}\cdot\hat{u}_A)^2 + \alpha^{-2}_{AB}(\hat{r}_{AB}\cdot\hat{u}_B)^2 - 2\chi_{AB}(\hat{r}_{AB}\cdot\hat{u}_A)(\hat{r}_{AB}\cdot\hat{u}_B)}{1 - \chi_{AB}^{2}(\hat{u}_A\cdot\hat{u}_B)^2}\right]^{-1/2} \tag{5}$$

$$\epsilon_{AB}^{(1)}(\hat{u}_A, \hat{u}_B) = [1 - \chi_{AB}^{2}(\hat{u}_A\cdot\hat{u}_B)^2]^{-1/2} \tag{6}$$

and

$$\epsilon_{AB}^{(2)}(\hat{u}_A, \hat{u}_B, \hat{r}_{AB}) = 1 - \chi'_{AB}\left[\frac{(\alpha_{AB}'^{2}(\hat{r}_{AB}\cdot\hat{u}_A)^2 + \alpha_{AB}'^{-2}(\hat{r}_{AB}\cdot\hat{u}_B)^2 - 2\chi'_{AB}(\hat{r}_{AB}\cdot\hat{u}_A)(\hat{r}_{AB}\cdot\hat{u}_B)}{1 - \chi_{AB}'^{2}(\hat{u}_A\cdot\hat{u}_B)^2}\right] \tag{7}$$

In ref 10, the authors suggest a mixing rule to calculate, from the aforementioned sets $\mathbf{P}_A$ and $\mathbf{P}_B$, the combinations of the quantities χ_{AB} and α_{AB}, as appearing in eqs 5−7, that is

$$\chi_{AB}\alpha_{AB}^{2} = \frac{(\sigma_A^{ee})^2 - (\sigma_A^{ss})^2}{(\sigma_A^{ee})^2 + (\sigma_B^{ss})^2}; \quad \chi_{AB}\alpha_{AB}^{-2} = \frac{(\sigma_B^{ee})^2 - (\sigma_B^{ss})^2}{(\sigma_B^{ee})^2 + (\sigma_A^{ss})^2} \tag{8}$$

$$\chi_{AB}^{2} = \frac{[(\sigma_A^{ee})^2 - (\sigma_A^{ss})^2][(\sigma_B^{ee})^2 - (\sigma_B^{ss})^2]}{[(\sigma_B^{ee})^2 + (\sigma_A^{ss})^2][(\sigma_A^{ee})^2 + (\sigma_B^{ss})^2]} \tag{9}$$

To obtain the other quantities (e.g. ϵ^{0}_{AB} or μ_{AB}), since no combination rule of this kind was found in the literature, a Lorentz−Berthelot approach has been followed where possible, thus defining

$$\epsilon^{0}_{AB} = (\epsilon^{0}_{A}\epsilon^{0}_{B})^{1/2}; \quad \sigma^{0}_{AB} = \frac{1}{2}(\sigma^{0}_{A} + \sigma^{0}_{B}) \tag{10}$$

$$\mu_{AB} = \frac{1}{2}(\mu_A + \mu_B); \quad \nu_{AB} = \frac{1}{2}(\nu_A + \nu_B); \quad \xi_{AB} = (\xi_A\xi_B)^{1/2} \tag{11}$$

The three remaining quantities, namely $\chi'_{AB}\alpha_{AB}'^{2}$, $\chi_{AB}\alpha_{AB}'^{-2}$, and χ'_{AB}, were here derived by comparing the standard GB expressions[9] for χ' with eqs 8 and 9, found in the literature[10] for $\chi\alpha^2$, $\chi\alpha^{-2}$, and χ^2. These considerations have lead to the definitions

$$\chi'_{AB}\alpha'_{AB} = \frac{(\epsilon_A^{ss})^{1/\mu_A} - (\epsilon_A^{ee})^{1/\mu_A}}{(\epsilon_A^{ss})^{1/\mu_A} + (\epsilon_B^{ee})^{1/\mu_B}}; \quad \chi'_{AB}\alpha_{AB}'^{-2} = \frac{(\epsilon_B^{ss})^{1/\mu_B} - (\epsilon_B^{ee})^{1/\mu_B}}{(\epsilon_B^{ss})^{1/\mu_B} + (\epsilon_A^{ee})^{1/\mu_A}}; \tag{12}$$

$$\chi'_{AB} = \frac{[(\epsilon_A^{ss})^{1/\mu_A} - (\epsilon_A^{ee})^{1/\mu_A}][(\epsilon_B^{ss})^{1/\mu_B} - (\epsilon_B^{ee})^{1/\mu_B}]}{[(\epsilon_B^{ss})^{1/\mu_B} + (\epsilon_A^{ee})^{1/\mu_A}][(\epsilon_A^{ss})^{1/\mu_A} + (\epsilon_B^{ee})^{1/\mu_B}]} \tag{13}$$

Equations 12 and 13 correctly reproduce the standard GB interaction in the limiting case A = B. Furthermore, they also can be used to model the interaction between an anisotropic and a spherical site, i.e. a gGB-LJ pair. In fact, this has been done in the 5CB hybrid model, which will be further discussed.

The second term of eq 1, U_{AB}^{Q}, is a quadrupole−quadrupole contribution,[3,35] whose asymptotic expression *i*

$$U_{AB}^{Q} = \frac{3}{4}Q_AQ_B[1 + 2(\hat{u}_A\cdot\hat{u}_B)^2 - 5(\hat{u}_A\cdot\hat{r}_{AB})^2 - 5(\hat{u}_B\cdot\hat{r}_{AB})^2 - 20(\hat{u}_A\cdot\hat{u}_B)(\hat{u}_A\cdot\hat{r}_{AB})(\hat{u}_B\cdot\hat{r}_{AB}) + 35(\hat{u}_A\cdot\hat{r}_{AB})^2(\hat{u}_B\cdot\hat{r}_{AB})^2]/r_{AB}^{5} \tag{14}$$

where the orientational $\hat{u}_i$ (i = A, B) and intermolecular vectors $\hat{r}_{AB}$ have the usual meaning, and Q_i (i = A, B) is the quadrupole value of the ith interacting site. The model intermolecular potential E^{inter}, of a couple of molecules i and j, can be expressed by

$$E^{inter} = \sum_{A}^{N_i}\sum_{B}^{N_j}U_{AB}^{inter} \tag{15}$$

where U_{AB}^{inter} is given in eq 1, and N_i and N_j are the number of interaction sites of molecules i and j, respectively.

The gGB parameter arrays **P** as well as the molecular quadrupoles Q of all interaction sites were obtained by a least-squares fitting procedure, using as reference the dimer interaction PES (E^{FRM}) of biphenyl, *p*-terphenyl, *p*-quaterphenyl, and *p*-quinquephenyl. The latter has been obtained[18,19] from ab initio calculations through the FRM approach.[24,25] The fitting was carried out by minimizing the integral **I**

$$\mathbf{I} = \sum_{k}^{N_g} w_k[E^{FRM}(\boldsymbol{R}_k, \Omega_k) - E^{inter}(\boldsymbol{R}_k, \Omega_k)]^2 \tag{16}$$

where $\boldsymbol{R}_k$ and Ω_k are, respectively, the intermolecular vector and the reciprocal orientation vector of the dimer in the kth geometry, and N_g is the number of employed geometries. Finally, w_k is a Boltzmann-like weighting factor which takes the form

$$w_k = e^{-\alpha E^{FRM}_k} \tag{17}$$

The molecular flexibility is taken into account by making each gGB disk able to rotate around the *p*-*n*-phenyl long axis. Such rotations are driven by an intramolecular torsional potential (E^{intra}) expressed by

$$E^{intra} = \sum_{i}^{n-1}[\sum_{j}^{M_i}C_{ij}\cos(m_{ij}\phi_i)] \tag{18}$$

where n is the number of rings, M_i is the number of cosine functions used for ring i, and C_{ij} and m_{ij} the potential parameters. The angle ϕ_i is the torsional dihedral between two neighboring rings (namely i and $i + 1$). For all the members of the series, this intramolecular potential has been parametrized in a previous work[28] by fitting the torsional energy profiles arising from accurate DFT calculations. The C_{ij} and m_{ij} parameters are reported in Tables 2, 4, and 6 of ref 28.

5CB. The model adopted for the 5CB molecule is shown in the lower panel of Figure 1. The 5CB's biphenyl core has been represented with two gGB oblate ellipsoids, whereas the N and C atoms (labeled N and C_n, see Figure 1) of the cyano group have each been modeled with a LJ potential. Following a standard UA description, all methyl and methylene groups of the lateral aliphatic chain have been also modeled with a single spherical LJ site. In this case, the term "hybrid" indicates that the model is composed by both isotropic (LJ) and anisotropic (gGB) interaction sites. Furthermore, a point charge was added to every site, so that the intermolecular model potential of two molecules i and j can be expressed by

$$E^{\text{inter}} = \sum_{A}^{N_i^{\text{gGB}}} \sum_{B}^{N_j^{\text{gGB}}} U_{\text{AB}}^{\text{gGB}} + \sum_{A}^{N_i^{\text{LJ}}} \sum_{B}^{N_j^{\text{gGB}}} U_{\text{AB}}^{\text{gGB/LJ}} + \sum_{A}^{N_i^{\text{gGB}}} \sum_{B}^{N_j^{\text{LJ}}} U_{\text{AB}}^{\text{gGB/LJ}} + \sum_{A}^{N_i^{\text{LJ}}} \sum_{B}^{N_j^{\text{LJ}}} U_{\text{AB}}^{\text{LJ}} + \sum_{A}^{N_i^{q}} \sum_{B}^{N_j^{q}} U_{\text{AB}}^{\text{Coul}} \quad (19)$$

where N_i^{LJ}, N_i^{GB}, and N_i^{q} are the number of LJ spheres, gGB ellipsoids, and point charges of molecule i.

The interaction energy between the gGB ellipsoids, $U_{\text{AB}}^{\text{gGB}}$, has the same expression given for the polyphenyls in eq 2, while the LJ potential energy, $U_{\text{AB}}^{\text{LJ}}$, has been slightly modified by the introduction of an additional parameter ξ:

$$U_{\text{AB}}^{\text{LJ}} = 4\epsilon^0{}_{\text{AB}}\left[\left(\frac{\xi_{\text{AB}}\sigma^0{}_{\text{AB}}}{r_{\text{AB}} + \sigma^0{}_{\text{AB}}(\xi_{\text{AB}} - 1)}\right)^{12} - \left(\frac{\xi_{\text{AB}}\sigma^0{}_{\text{AB}}}{r_{\text{AB}} + \sigma^0{}_{\text{AB}}(\xi_{\text{AB}} - 1)}\right)^{6}\right] \quad (20)$$

This has been done both to increase the flexibility of the function in the fitting procedure and to make it consistent with the expression of the gGB potential, $U_{\text{AB}}^{\text{GB}}$, given in eq 2. As done for the polyphenyl series, the three quantities $\sigma^0{}_{\text{AB}}$, $\epsilon^0{}_{\text{AB}}$, and ξ_{AB} can be computed from the parameters specifying each site (i.e. $\sigma^0{}_i$, $\epsilon^0{}_i$, and ξ_i, with i = A, B) through the following mixing rules

$$\epsilon^0{}_{\text{AB}} = \sqrt{\epsilon^0{}_{\text{A}}\epsilon^0{}_{\text{B}}};\ \sigma^0{}_{\text{AB}} = \frac{\sigma^0{}_{\text{A}} + \sigma^0{}_{\text{B}}}{2};\ \xi_{\text{AB}} = \sqrt{\xi_{\text{A}}\xi_{\text{B}}} \quad (21)$$

The hybrid interaction term $U_{\text{AB}}^{\text{gGB/LJ}}$, between an anisotropic gGB site A (B) and a spherical LJ one B (A), can also be described, as previously stated, by eq 2. Indeed, due to its spherical symmetry, the following relations stand for the ith (i = A, B) LJ site:

$$\sigma_i^0 = \sigma_i^{\text{ee}} = \sigma_i^{\text{ss}};\ \epsilon_i^0 = \epsilon_i^{\text{ee}} = \epsilon_i^{\text{ss}};\ \mu_i = \nu_i = 1 \quad (22)$$

In eqs 5−7, defining σ_{AB}, $\epsilon_{\text{AB}}^{(1)}$ and $\epsilon_{\text{AB}}^{(2)}$, this implies the annealing of the coefficients of the terms formally depending on the orientational vector $\hat{u}_i$ of the isotropic LJ site. For instance, in the interaction between a LJ site A and a gGB one B, eq 5 defining σ_{AB} simply reduces to

$$\sigma_{\text{AB}}(\hat{u}_{\text{B}}, \hat{r}_{\text{AB}}) = \sigma^0{}_{\text{AB}}[1 - \chi_{\text{AB}}\alpha_{\text{AB}}^{-2}(\hat{r}_{\text{AB}}\hat{u}_{\text{B}})^2]^{-1/2}$$

As one can see, this term correctly depends only on the distance vector between the isotropic (A) and the anisotropic (B) interaction site, $\hat{r}_{\text{AB}}$, and on the anisotropic site orientation, $\hat{u}_{\text{B}}$. Finally, the point charges interaction term $U_{\text{AB}}^{\text{Coul}}$ has been computed by a standard Coulomb potential.

The parametrization of the 5CB hybrid intermolecular potential has been carried out with the same procedure described, for the oligophenyl series, by eq 16. The reference ab initio PES for the dimer was already computed through the FRM approach and was recently[25] employed in an atomistic modeling of 5CB. The molecular flexibility of the 5CB molecule is certainly more complex than the polyphenyls one. Its description has been carried out by the intramolecular term E^{intra}, which results in a sum of stretching, bending, torsional, and intramolecular LJ contributions:

$$E^{\text{intra}} = E^{\text{stretch}} + E^{\text{bend}} + E^{\text{tors}} + E^{\text{LJintra}} \quad (23)$$

For all the terms in the above sum, the standard AMBER[36] expressions have been adopted. The parametrization of such potential terms for 5CB has been recently made by our group on the base of accurate quantum mechanical calculations,[26] and successfully validated through lengthy molecular dynamics simulations,[26,34] performed with the aforementioned atomistic modeling. All parameters of stretching, bending, and torsional intramolecular potentials can be found in Tables 1−5 of ref 26.

2.2. Computer Simulations. All simulation runs were carried out with the Monte Carlo method[37] (MC). To study phase transitions, the isothermal isobaric ensemble (NPT) has been preferred to the canonical one (NVT), although a bit computationally more expensive. In fact, MC NPT techniques, allowing fluctuations of the shape and the volume of the simulation box, favor the achievement of the natural structure of the system. Furthermore, the NPT ensemble is the closest to experimental conditions, since real experiments are usually performed at constant pressure.

The short-range intermolecular interactions have been truncated at R_c = 10 Å, employing the energy standard correction.[38] In the 5CB system, charge−charge long-range interactions have been treated with the Ewald method,[39] using a convergence parameter α of $5.36/2R_c$. All MC runs have been performed according to the usual rules of the NPT scheme, using systems of 600 molecules for the oligophenyl series and 192 for the 5CB simulations. The latter number has been chosen both for computational convenience and for a better comparison with the results of the previous atomistic model.[25] During the runs a molecule was selected at random, and trial displacements of its center of mass and inertia axes were performed. To sample the intramolecular

conformational space, a randomly selected gGB disk could also be rotated around the molecular long axis of both oligophenyls and 5CB. Moreover, for 5CB, attempts to move the chain's interaction sites were also performed, so to alter their stretching, bending, and torsional coordinates. Finally, the shape and the volume of the computational box have been changed during simulations, by attempting to vary a randomly selected edge of the box. With the aim of preserving the detailed balance condition, all the aforementioned trial moves have been selected randomly and not sequentially.

The equilibration of the systems studied has been assessed by monitoring the evolution of a number of observables such as enthalpy, density, and orientational order parameter, P_2. The latter was obtained by diagonalizing the Saupe ordering matrix **Q**, whose elements are defined as

$$Q_{ab} = \left\langle \frac{1}{2}(3u_a u_b - \delta_{ab}) \right\rangle$$

where the mean value $\langle \ldots \rangle$ is obtained averaging on all molecules composing the system, and $\hat{u}$ ($a = x, y, z$) is the eigenvector corresponding to the minimum eigenvalue of the molecular inertia tensor, i.e., the long principal axis. The maximum eigenvalue of Q is then taken as the principal order parameter P_2, and the corresponding eigenvector represents the phase director **n**.

Every equilibration has been followed by a production run for the evaluation of the thermodynamic properties. Positional order was monitored by calculating the correlation functions $g(r)$, $g(r_{\parallel})$, and $g(r_{\perp})$. $g(r)$ is the standard isotropic correlation function, while $r_{\parallel}$ and $r_{\perp}$ are the projections of the center of mass vectors along and normal to **n**, respectively. The orientational order was studied calculating the major order parameter P_2 and the orientational correlation function $G_2(r)$.[40] This function, computed as

$$G_2(r_{ij}) = \langle P_2(\hat{u}_i \cdot \hat{u}_j) \rangle (r_{ij})$$

describes the orientational correlation of two molecules *i* and *j* as a function of the distance between their center of mass. As shown by Bates et al.,[41] $G_2(r)$ reaches the asymptotic value of $\langle P_2 \rangle^2$ at large r_{ij}.

3. Results and Discussion

***p*-Polyphenyls.** The intermolecular PES of the *p*-*n*-phenyls have been computed through the FRM method,[24] which is based on the construction of a dimer interaction potential as a sum of fragment−fragment contributions. In particular, the polyphenyls PES can all be obtained as a sum of benzene−benzene interaction energies. The details of these FRM calculations have been already reported in refs 18 and 19. Furthermore, the accuracy of the ab initio calculations on the benzene dimers has been also extensively discussed in previous works.[24,42,43]

The computed *p*-*n*-phenyls PES have been fitted with the gGB model potential, reported in eq 1. In view of the poor significance of very repulsive values, all the energies $E_k^{\mathrm{FRM}} > 80$ kJ/mol were discarded from the integral **I** of eq 16, and the weighting coefficient α, defined by eq 17, was set to 0.84 (kJ/mol)$^{-1}$. Preliminary fittings performed over a wide α interval (0.42 (kJ/mol)$^{-1}$ < α > 8.37 (kJ/mol)$^{-1}$) showed a negligible dependence of the shape of the fitted curves over the weighting factor, at least in the considered conformations. Finally, the parametrization conforms to the molecular symmetry, i.e. equivalent rings are represented by identical gGB and quadrupolar potential terms. The obtained parameters are reported for all the series in Tables 1 and 2.

Table 1. Parameters of the GGB Model for the Oligophenyl Series[a]

n	*m*	ϵ_0	ϵ_{ss}	ϵ_{ee}	σ_0	σ_{ss}	σ_{ee}	μ	ν	ξ
2	1,2	1.26	4.18	28.38	6.83	6.83	3.18	1.0	1.20	0.86
3	1,3	1.59	5.02	13.60	6.69	6.69	3.41	1.0	2.07	0.89
3	2	0.71	1.80	48.03	6.86	6.86	2.83	1.0	−0.87	0.77
4	1,4	1.34	5.82	47.15	6.90	6.90	3.20	1.0	−0.86	0.83
4	2,3	1.67	2.34	22.13	6.56	6.56	3.16	1.0	−0.61	0.84
5	1,5	1.34	2.89	35.90	6.85	6.85	3.21	1.0	−1.24	0.79
5	2,4	2.26	2.34	25.06	6.51	6.51	3.19	1.0	−3.42	0.83
5	3	1.21	5.86	34.02	6.43	6.43	3.31	1.0	1.46	0.81

[a] *n* indicates number of phenyl rings in the molecule, and *m* indicates the position of the ring inside the polyphenyl; ϵ's are in kJ/mol and σ's in Å.

Table 2. Optimized Quadrupoles of the gGB Model for the Oligophenyl Series[a]

n	*Q*	SD	*n*	*Q*	SD
2	15.6	2.68	4	13.3	2.51
3	18.1	1.97	5	10.4	2.68

[a] All quadrupoles were imposed to be equal on each phenyl ring and are reported in C · m^2 · 10^{40}; in the last column, the standard deviations of the fitting procedures are reported in kJ/mol for each polyphenyl.

As it can be seen from the standard deviations reported in Table 2, although based on a reduced number of interaction sites with respect to an atomistic model, the present gGB model can describe to a good level of accuracy the main features of the reconstructed ab initio PES.

In Figure 2, cross sections of the computed FRM-PES are compared with the fitted potential for some selected conformations of *p*-quinquephenyl. In the first panel from the left, a sandwich parallel conformation is obtained by displacing the center of mass of one molecule along the translation vector ***R*** perpendicular to the central ring plane. All other conformations (i.e. cross, parallel displaced and T-shaped) are shown in the other panels of Figure 2 together with the selected ***R***. Similar results have been obtained for the other members of the series. It might be noted that aligned conformations (first and third panels from the left in Figure 2) result in deeper wells, thus favoring orientationally more ordered geometries. It may be worth also noticing as in the parallel displaced curve (third panel from the left), the model quadrupolar interaction allows for reproduction of the shift of the minimum toward slipped configurations ($R > 0$), found by the quantum mechanical results.[18]

Preliminary MC runs on the *p*-*n*-phenyls series had already been performed by our group,[19] by coupling the fitted intermolecular PES to a torsional ring−ring potential reported in the literature.[44] Unfortunately, it turned out that the height of the barrier for the planar conformation of biphenyl in ref 44 was overestimated compared to more recent experimental

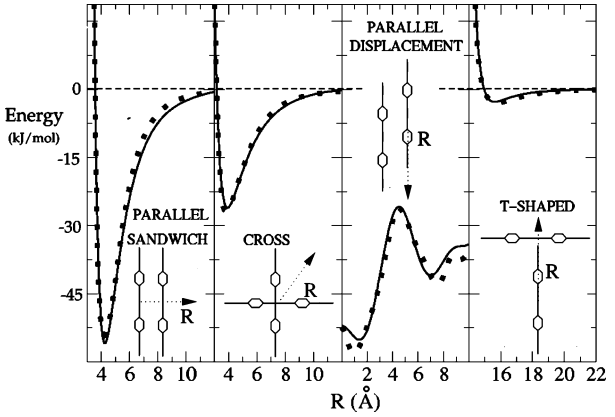

Figure 2. Selected cross sections of the FRM intermolecular PES (dotted black line) and the fitted gGB model (solid black line) for the polyphenyls series. The translation vector **R** is reported in the inner panels, for each of the considered geometries, with a dotted arrow. In the middle panels, the latter is perpendicular and parallel to both molecular long axis in cross and parallel displaced geometries, respectively. The intermolecular distance *R* is reported in Å and all energies in kJ/mol.

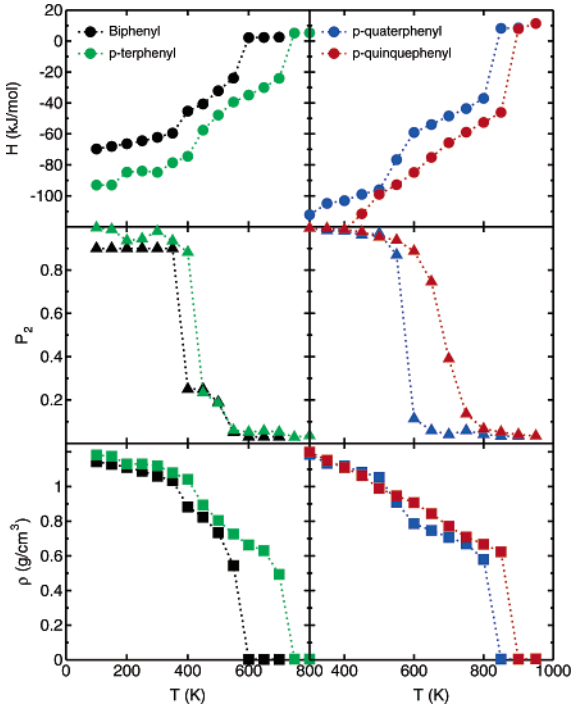

Figure 3. Thermodynamic properties of *p-n*-polyphenyls as a function of temperature for biphenyl (black symbols, left panels), *p*-terphenyl (green symbols, left panels), *p*-quaterphenyl (blue symbols, right panels), and *p*-quinquephenyl (red symbols, right panels). Enthalpies (circles) are in kJ/mol and densities (squares) in g/cm^3. All values have been averaged over production runs of 50 · 10^6 MC steps.

and theoretical data.[45,46] This led to inaccurate predictions of the thermodynamical properties of all the series.[19] In this work, MC NPT runs have been performed using the intermolecular hybrid model coupled with the intramolecular torsional potential reported in ref 28.

All simulations were started from the same configuration, created for all the omologues according to the following procedure. The polyphenyl centers of mass were disposed in a fcc crystal structure, elongated in the [111] direction, and chosen parallel to the *z* axis. Their molecular long axes were all aligned along the *z* direction, thus yielding a starting order parameter $P_2 = 1$; the dihedral angles between two contiguous disks were set to ∼45°, which corresponds to the minimum of the torsional potential as calculated in ref 28. Next, all crystals were expanded to a density $\rho \simeq 0.8$ g/cm^3, to favor the disordering processes. Starting from this expanded crystal, several MC runs were performed on each omologue at atmospheric pressure and varying the temperature by 50 K steps.

In Figure 3 the enthalpy, density, and orientational order parameter P_2 are shown as a function of temperature for the four systems. Some of the thermodynamical results reported in Figure 3 are compared with experimental data in Table 3.

The melting points (T_m) were determined in simulation by considering the average value between the highest temperature in the solid and the lowest in the liquid phase for each oligophenyl; clearing (T_{NI}) and boiling (T_b) points were determined analogously. In this way the computed values carry an uncertainty of ±25 K. At low temperatures, the four systems show a translationally and orientationally ordered phase. Raising the temperature, a liquid and a gas phase appear, with an almost vanishing orientational order parameter P_2, but with definitely different enthalpies and densities. With regards to the 5 ring member, a third fluid phase was found, with a partial orientational order ($P_2 \simeq$ 0.7). The lack of positional ordering, associated with a $P_2 > 0.4$, is typical of a nematic phase. The latter is experimentally found for *p*-quinquephenyl between 653 and 681 K,[49] thus very close to the computed range (625−675 K). In fact, Table 3 shows that the adopted model, although coarse grained, is capable of reproducing the range of stability of the phases with an error of ≃50 K. On the contrary, all transition enthalpies are significantly underestimated, with relative deviations increasing along the series.

Table 3. Thermodynamic Results of the Employed Hybrid Model[d]

n	T_m	T_{NI}	T_b	ΔH_m	ΔH_{NI}	$\Delta H°_{vap}$
2	375		575	14.2		27.4
	344[a]		529[b]	18.8[a]		54.0[b]
3	425		725	17.1		34.6
	493[a]		658[b]	35.4[a]		79.0[b]
4	575		825	17.7		56.7
	587[a]		773[b]	37.8		117.0[b]
5	625	675	875	11.4	7.9	65.1
	660[a]	688[a]	823[b]	42.3[a]	0.9[a]	151.0[b]
	653[c]	681[c]				

[a] Reference 47. [b] Reference 48 and references therein. [c] Reference 49. [d] *n* indicates the number of phenyl rings in the *p-n*-phenyls. All temperatures are in K; all ΔH's are in kJ/mol.

The ordered phase shown at 650 K by *p*-quinquephenyl has been analyzed in more detail. First, in view of the known tendency of these systems to remain trapped in metastable states, the runs at $T = 600$, 650, and 700 K have been

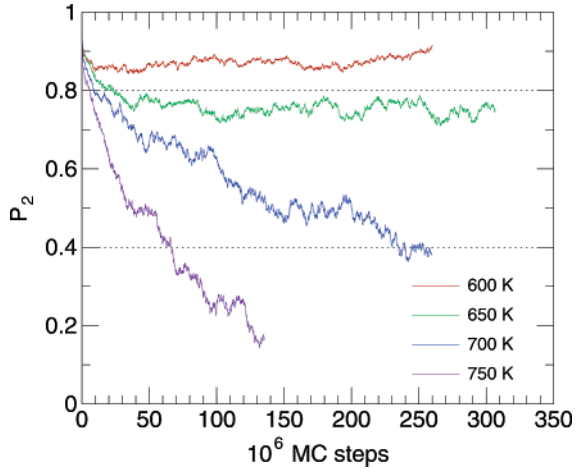

Figure 4. Equilibration of the order parameter of the *p*-quinquephenyl molecule at different temperatures. The nematic range [0.8−0.4] is indicated between dotted lines.

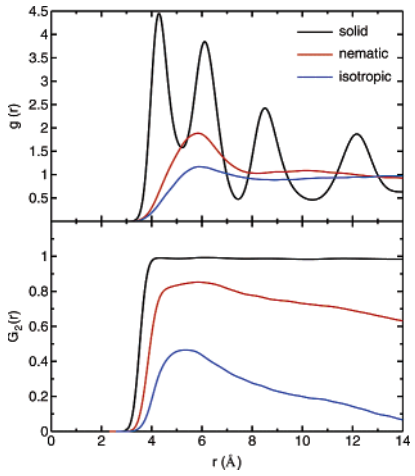

Figure 5. Correlation functions for *p*-quinquephenyl in the crystal (black line), in the nematic (red line) and liquid phase (blue line) at $T = 350$, 650, and 800 K respectively.

extended to over $250 \cdot 10^6$ MC steps. The P_2 was plotted over the step number and reported in Figure 4. The order parameter at 650 K (green line) remains stable for about 200 million configurations, resulting in an average value of $P_2 = 0.74$, whereas it grows up to 0.9 at 600 K (red line), and it falls under 0.4 (blue line) if the temperature is raised to 700 K. To assess the nematic nature of the phase at 650 K, the pair correlation functions $g(r)$ and $G_2(r)$ have been computed and reported in Figure 5. From the upper panel, it can be seen that, despite the high orientational order, no positionally ordered structure is present at 650 K, and the $g(r)$ correlation function shows a shape very similar to the one computed in the isotropic liquid phase. The $G_2(r)$ function at 650 K shows a long-range correlation, which decays to the expected $\langle P_2 \rangle^2$ value, consistent with the nematic nature of the orientationally ordered phase.

The proposed model accounts for flexibility through the intramolecular torsional potential computed in ref 28. The validation of the latter could be assessed if the proposed model results are able to reproduce the delicate interplay between intermolecular and intramolecular forces that drive

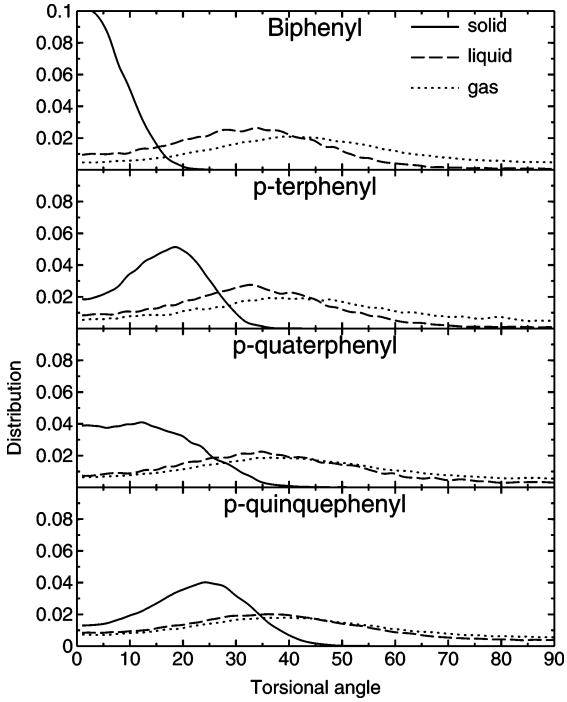

Figure 6. Population distribution of the first torsional angle along the *p*-oligophenyls series. For all molecules, distributions in solid, liquid, and gas phases are reported with solid, dashed, and dotted lines, respectively.

the phase transitions in the *p*-oligophenyls series. Indeed, the experimental inter-ring angle of biphenyl results to be around 40° in gas phase,[50,51] 32° in liquid phase,[52] and nearly 0° in crystalline phase.[53] This tendency is apparent also in the larger homologues,[54] where the molecular planarity is lost in going from the crystalline to the less ordered structures. In fact, this experimental trend is well reproduced by the simulation data, as one can see from Figure 6, where the distribution functions of the first dihedral angle are reported at different temperatures. For all the members of the series, a neat change in population can be observed at the transition between crystalline and liquid phases, in agreement with the experimental findings.[54] This can be easily explained by considering the gain in intermolecular energy due to the closer packing allowed for the planar conformations. Furthermore it is worth noticing the importance for the model to account for an accurate representation of internal flexibility. Indeed, the correction of the aforementioned overestimation in the torsional potential adopted in the preliminary runs[19] adjusts the balance between intermolecular and intramolecular contributions, thus leading to more accurate thermodynamic results, including transition temperatures. For instance, the melting temperatures of *p*-terphenyl and *p*-quaterphenyl for the present model are 425 and 575 K, respectively. These values clearly show a better agreement with the experimental measures (493 and 587 K[47]) with respect to those found in the preliminary runs,[19] namely 375 and 475 K.

5CB. The 5CB intermolecular potential energy surface, previously computed by the FRM method,[24,25] was fitted into the hybrid GB/LJ model. The fitting procedure, performed according to eq 16, has already been applied in ref 25 to an

Table 4. Fitted Intermolecular Parameters for the 5CB Hybrid Model[a]

site	ϵ_0	σ_0	ξ	ϵ_{ss}	ϵ_{ee}	σ_{ss}	σ_{ee}	μ	ν	q
Bz1	2.22	6.23	0.86	5.40	25.19	6.23	2.89	1.41	2.87	−0.070
Bz2	2.47	6.46	0.72	3.93	25.56	6.46	3.14	1.13	−1.02	0.127

	ϵ_0	σ_0	ξ	q
N	0.02	3.21	0.68	−0.369
Cn	0.07	2.68	0.15	0.318
Cp1	1.00	2.49	1.42	0.024
Cp2	0.33	4.16	0.70	0.000
Cp5	0.02	4.58	1.38	−0.030

[a] The charge on Cp2 site was imposed to be null. All ϵ's are reported in kJ/mol, σ's in Å, and all charges in fraction of e.

atomistic model potential. This 5CB atomistic model was used[26,34] in molecular dynamics (MD) simulations, and it was shown to reproduce with good approximation the thermodynamic, structural, and dynamic properties of 5CB crystalline, nematic, and liquid phases. In the present work, in fact, during both the parametrization and the validation procedures, the obtained results will be compared with those reported for the more "realistic" atomistic model.

Here, as done for the latter,[25] all repulsive energies larger than 40 kJ/mol were discarded from the sample of $N_g \simeq 2 \times 10^4$ dimer conformations, and the weighting coefficient α was set to to 1.67 $(kJ/mol)^{-1}$. Furthermore, the partial charges on the three Cp2 sites were imposed to be null, and their parameters were taken as equivalent. No other restriction but electroneutrality was imposed, obtaining in such a way a standard deviation of 2.8 kJ/mol. The latter well compares with the one obtained for the atomistic model,[25] i.e. 2.5 kJ/mol. The resulting intermolecular parameters are reported in Table 4.

Other coarse grained parametrizations, performed on biphenyl[18,19] or on cyanobiphenyl in 5CB,[20] report a strong dependence of the fitted parameters on the chosen weighting factors. In particular in ref 20, where a uniaxial single GB site is employed to model the cyanobiphenyl moiety in 5CB, the GB radii (σ_{ss} and σ_{ee}) are found to be very sensitive to the temperature employed in the fitting. In the present work, the value of the employed weighting factor α corresponds to a temperature of ≃200 K. As reported for the *n*-phenyls, other fittings performed with α set to 0.42 $(kJ/mol)^{-1}$ and 8.37 $(kJ/mol)^{-1}$ (corresponding to temperatures of 50 and 1000 K, respectively) did not show relevant differences in the shapes of the coarse grained PES. For instance, in the face-to-face conformation of the 5CB dimer (see Figure 7), the well depth (≃ −40 kJ/mol with $\alpha = 1.67$ (kJ/mol^{-1})) showed variations of less than 5%, while the distance where the fitted curves cross the $y = 0$ axis changes with α only by ≃2%. This different behavior with respect to other coarse grained parametrizations probably arises from the more accurate level of approximation introduced by the present model. Indeed, substituting each phenyl ring with a rigid gGB site implies only the remotion of "hard" internal potentials, which rule the ring hexagonal shape and planarity. Therefore, the degrees of freedom neglected by this model do not change much with temperature in the real molecule. Conversely, the substitution of both rings with a single (prolate) GB site[18,20]

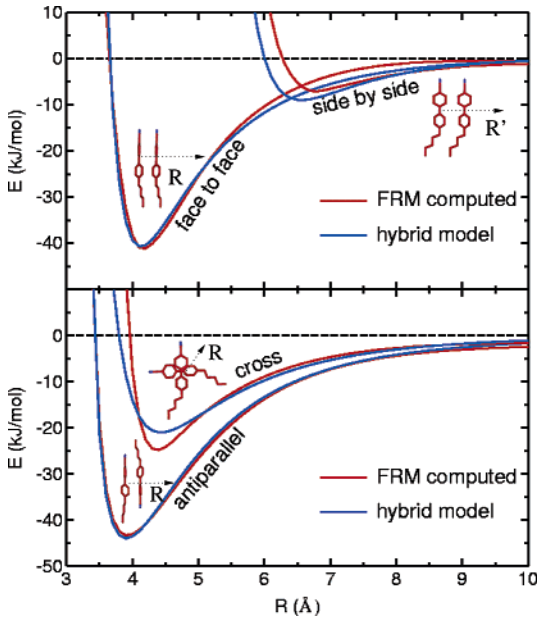

Figure 7. FRM reconstructed (red line) and hybrid model potential (blue line) energy curves. Translation vectors $\hat{\boldsymbol{R}}$ and $\hat{\boldsymbol{R}}'$, defined in the text, are reported in the inner panels with dotted black arrows. Energies are in kJ/mol and distances are in Å.

also removes the inter-ring "soft" potential, which drives molecular biaxiality and shows a rather flat shape in the minimum region.[28,25] In this case,[18,20] a rotational average on the reference PES is needed before performing the fitting, thus introducing the reported strong temperature dependence.

As done for the *p*-*n*-phenyls, some fitted potential curves are compared in Figure 7 with the corresponding FRM reconstructed energies, for selected dimer arrangements. The latter have been constructed as follows. In the parallel conformations, reported in the upper panel of Figure 7, the second molecule is moved along a vector **R** containing the midpoint of the ring−ring linkage, parallel to the $\hat{C}_6$ symmetry axis of the cyanophenyl group for the face-to-face geometries. The side-by-side arrangements are obtained by translating the second molecule along the vector **R′** containing the ring−ring linkage and perpendicular to both the molecular long axis and the $\hat{C}_6$ symmetry axis. In the antiparallel and cross geometries (lower panel of Figure 7), a rotation of 180° and 90°, respectively, is performed around $\hat{R}$, together with a translation along it. The agreement for all the four considered configurations is good; in particular the local parallel and antiparallel minima are well represented.

It is also worth noticing that the parallel dimer conformation is correctly less favorite than the antiparallel one. This is mainly due to the repulsive Coulomb contribution, which can be ascribed to an unfavorable dipole−dipole parallel arrangement. Indeed, the Coulomb contribution to the energy of the hybrid model in the parallel and antiparallel local energy minima result +7.1 kJ/mol and −0.1 kJ/mol, respectively. Moreover in the latter geometry, it may be of some interest to investigate the source of all energy contributions which concur to the local minimum and to compare the distribution arising in both the FRM calculation and the fitted hybrid model. The core−core, core−chain, and chain−chain

Table 5. FRM[24] and Fitted Energy Contributions in kJ/mol in the Antiparallel Local Energy Minimum

	FRM[24]	hybrid fitted model
r_0 (Å)	3.9	3.9
total energy	−43.4	−43.7
core−core	−33.6	−33.5
core−chain	−8.5	−9.6
chain−chain	−0.2	−0.5
Coulomb		−0.1

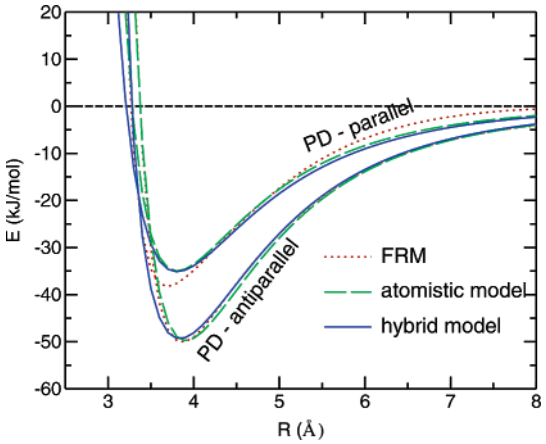

Figure 8. Comparison between FRM (red, dotted line) curve and atomistic[25] (green dashed line) and hybrid (blue solid line) models for some selected parallel displaced (PD) conformations. Energies are in kJ/mol and distances are in Å.

FRM terms, reported in Table 5, can be easily computed as sums of the appropriate fragment−fragment contributions. The core−chain term, for instance, arises from the sum of all benzonitrile−pentane and benzene−pentane interaction energies. Conversely, in the fitted model, the three contributions arise from different types of interactions: gGB-gGB, gGB-LJ, and LJ-LJ, respectively.

From the quantities reported in Table 5, it is evident that the hybrid model is capable of conserving the correct distribution of the energy contributions found by the FRM approach.[24] In fact it can be seen that the main source of attraction is the interaction between the aromatic cores, which accounts for almost 80% of the total interaction energy.

Finally, in Figure 8 a comparison between the 5CB atomistic[25] and hybrid models is presented. Two parallel displaced (PD) conformations were created with the same procedure, i.e. a displacement along the long molecular axis of 5.0 Å and −2.5 Å for the parallel and antiparallel dimers, respectively. The agreement between the two models is satisfactory, as the hybrid models do not lose much accuracy in representing the FRM curves, with respect to the more "realistic" atomistic one.

5CB simulations were carried out in the NPT ensemble, making use of the hybrid GB/LJ intermolecular model coupled to the intramolecular potential whose parametrization has been described in detail in ref 26.

Two configurations of 192 molecules, in the nematic and isotropic phase respectively, were extracted from the equilibrated trajectories of MD simulations previously performed by our group with the 5CB atomistic FRM model.[25,26,34]

Table 6. Calculated and Experimental Thermodynamic Properties[a]

	this work	MD-FA[26]	exp
ρ (300 K)	1.092 ± 0.04	1.085 ± 0.03	1.020[55]
ρ (320 K)	1.051 ± 0.05	1.063 ± 0.04	0.995[55]
P_2 (300 K)	0.546 ± 0.01	0.538 ± 0.03	0.54[56]
P_2 (320 K)	0.151 ± 0.01	0.176 ± 0.03	
U_{inter} (300 K)	−98.4 ± 0.1	−106.9 ± 0.5	
U_{inter} (320 K)	−86.7 ± 0.1	−103.7 ± 0.7	
CPU time/step	0.02	0.6	
$N_{steps} \cdot 10^6$	220	40	

[a] The data of this work, averaged over 50 millions MC steps, are compared with the corresponding MD values, reported in ref 26. Density ρ is expressed in g/cm^3, and intermolecular energies contributions U^{inter} are in kJ/mol. In the last two rows are reported the CPU time/step in seconds and the average number of steps needed to reach equilibrium, N_{steps}. Both MC and MD calculations were performed on Xeon 2.8 GHz processor.

These geometries were expanded to a density of 0.8 g/cm^3, and the interaction sites (six aromatic carbons and four hydrogens) of each phenyl ring were substituted with a rigid gGB disk, centered in the geometrical center of the phenyl plane and with its orientation axis $\hat{u}_{gGB}$ perpendicular to the ring (see panel b of Figure 1). Such hybrid configurations were eventually used as starting point for two MC-NPT runs at atmospheric pressure, at 300 and 320 K.

Equilibration, assessed by monitoring total energy, density, and order parameter of both systems, was reached after ≃280 $\cdot$ 10^6 and 160 $\cdot$ 10^6 MC steps for the lower and higher temperature, respectively. A comparison of the CPU usage of these simulations, with respect to the atomistic MD runs performed on the same system,[26,34] cannot be easily carried out, since different techniques as well as different modeling levels are concerned.

Nevertheless, in the last row but one of Table 6, the CPU time/step has been reported for the two methods. The cost of the MD technique is not surprising, considering that each step involves a collective move, the calculation of the forces, and the computation of the energies for a larger number of interaction sites. However, in the discussion of the CPU usage with the two different techniques, the number of steps performed to reach equilibrium should be also taken into account. The latter quantity has been reported in the last row of Table 6 and clearly shows the better efficiency of MD steps to reach equilibrium.

Once equilibrated, production runs of 50 $\cdot$ 10^6 MC steps have been carried out for both temperatures. The values of some average quantities are reported in the first rows of Table 6 and compared with those obtained with the atomistic MD runs. These results seem to indicate that the adopted hybrid model is still capable of reproducing stable isotropic and nematic phases in the experimental temperature range. In particular the orientational order parameter in the nematic phase at 300 K well agrees with both the MD and the experimental value. Conversely, by looking at the first rows of Table 6, one may note as the gain in energy from the isotropic phase at 320 K to the nematic at 300 K is higher for the hybrid model (11.7 kJ/mol) than for the atomistic one (3.2 kJ/mol), which better compares with the experimental clearing enthalpy ΔH^c of 0.54 kJ/mol.[57] Accordingly,

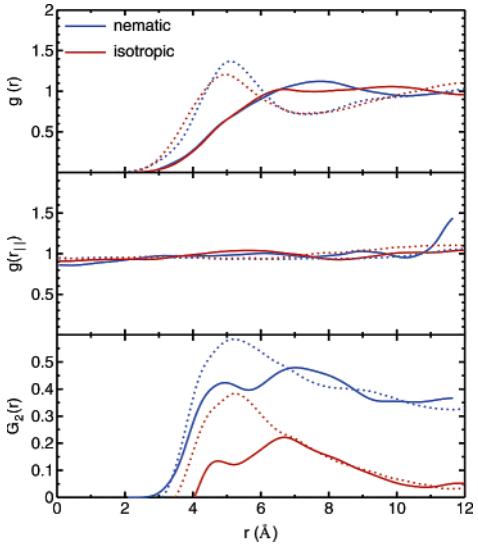

Figure 9. Correlation functions in the nematic (300 K, blue lines) and isotropic (300 K, red lines) phases. MC results of this work are reported with solid lines, while dashed lined are used for MD results of ref 26.

the MC ordered system at 300 K increases its density with respect to the MD value, while the isotropic phase behaves in an opposite manner.

A more detailed characterization of the structure of the two resulting condensed phases can be obtained from the computed correlation functions, $g(r)$, $g(r_{||})$, and $G_2(r)$, reported in Figure 9.

As can be seen from the behavior of $g(r)$ and $g(r_{||})$ functions (solid lines in Figure 9), no positional order is present in the two phases and both exhibit a liquidlike structure. More importantly, the $G_2(r)$ orientational correlation function at 300 K correctly decays to an asymptotic value of $\simeq$0.33, which is consistent with $\langle P_2\rangle^2 = 0.3$, thus confirming the nematic nature of the condensed phase at lower temperature. The $g(r)$ functions for the atomistic model[25,26] (reported with dashed lines) show a different short-range structure with respect to the hybrid model results. This is rather surprising since both models were fitted on the same FRM PES, and they show (see Figure 4) a very similar behavior, at least on the investigated configurations. Indeed, this extreme sensibility of the simulated properties of complex materials to the details of the molecular interactions reinforces the need of specifically computed intermolecular PES as well as models potential capable of accurately reproducing them.

Another important feature to verify is the capability of the hybrid coarse grained model to reproduce the molecular flexibility of the 5CB molecules. In Figure 10 are reported population distributions of the inter-ring dihedral (δ) and the first dihedral of the aliphatic chain (ϕ), i.e. defined by the sites Bz2-Cp1-Cp2-Cp2 (see Figure 1, panel b). With regards to the former, the average value of the dihedral between the two gGB disks 32.6° in the nematic phase well agrees with both experimental[56] (37°) and the atomistic model[26] results (31°). The distribution of conformers in the aliphatic chain, monitored by the dihedral ϕ, confirms the tendency of the 5CB molecules to assume a more elongated geometry in the

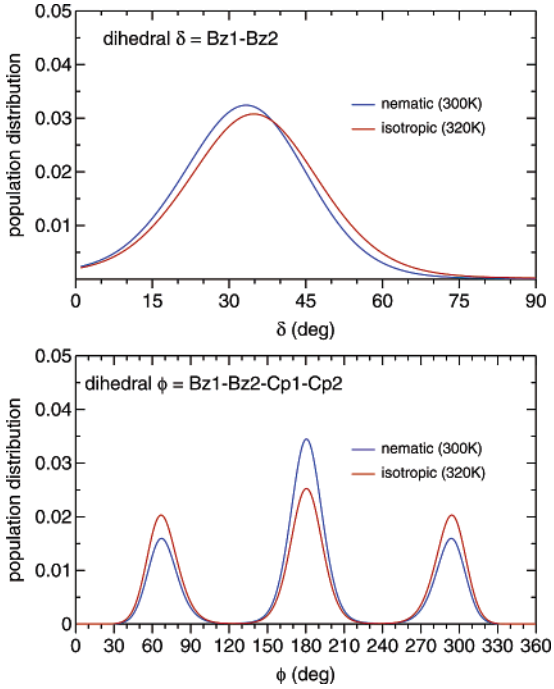

Figure 10. Population distribution functions of the inter-ring dihedral δ (upper panel) and the first chain torsional dihedrals ϕ (bottom) in the nematic (blue lines) and isotropic (red lines) phases.

nematic phase, by increasing the trans population with respect to the gauche one. This is in good agreement with both the experimental[56] findings and the atomistic model results.[26]

4. Summary and Conclusions

In this paper, coarse grained hybrid potentials, suitable for computer simulations of advanced materials, have been parametrized and validated through MC computer simulations. Thanks to the FRM approach,[24,25] pair potentials of large molecular dimers can be ab initio computed, constructing a reference PES on which the hybrid models can be sewn. In this way, the chemical detail entailed in a quantum mechanical description can be transferred, up to the chosen level of accuracy, to rather simple models that can be used in computer simulations. It may be worth stressing that the FRM/coarse grained approach can be employed for any large molecular system. Once obtained, the transferability of the FRM-derived parameters must be carefully evaluated in each case: in the polymer field, for instance, simulations of polyphenylene or similar molecules could be tempted with the adoption of the many gGB disks model, without the need of further parametrizations. Conversely, the specificity of the FRM derived potentials can become a drawback if one tries to extend the use of the same coarse grained parameters to similar fragments in very different chemical backgrounds.

In the cases studied, the proposed models have proven capable of reproducing the computed FRM PES with good approximation. The augmented tendency of the larger homologues of the *p*-*n*-phenyl series to assume parallel conformations is well reproduced by the gGB disks as well as the effect of the ring quadrupoles to shift the minimum energy toward displaced conformation. With regards to the

5CB molecule, comparison with the more realistic full atomic potential,[25,26] fitted on the same FRM PES, shows that most of the features of the molecular interaction are correctly accounted for. In a hierarchy of simulation models, the realism and computational complexity of such hybrid potentials lies between a single-site representation[3,7] and a fully atomistic modeling. Notwithstanding their simplicity, the proposed models have been proven capable of describing at the semiquantitative level the phase diagram of the *p*-oligophenyl series and reproducing to a good level of accuracy the structure and orientational properties of a typical mesogen.

Among the formers, three phases (solid, liquid, and gas) were reproduced at atmospheric pressure for the $n < 5$ members, with a maximum error of ≃50 K on the phase transition temperatures. Furthermore, the larger homologue, namely *p*-quinquephenyl, showed an orientationally ordered phase ($P_2 \simeq 0.7$) at 650 K and 1 atm, not far from the experimental range (653−688 K[47,49]). Conversely, the transition enthalpies are underestimated if compared with the relative experimental values, with an increasing error for the larger homologues. This might be due to the lack of intramolecular flexibility of the hybrid model, which neglects all internal degrees of freedom except the torsion between adjacent rings. Indeed, the importance of molecular flexibility on the resulting bulk properties is confirmed by the increased accuracy of the present results with respect to those obtained, for the oligophenyl series, by the use of single site models[18,19] or less accurate intramolecular potentials.[19] The inclusion (and the accurate description) of "flexible" internal coordinates appears to be a necessary feature for an accurate representation of the phase transitions. The hybrid model adopted for the 5CB molecule was shown to be able to reproduce a nematic and an isotropic liquid phase, in the correct temperature range. Both these phases, however, showed a short-range structure noticeably different from that shown by the correlation functions obtained[26] for the more realistic atomistic model. On the contrary, the internal distribution of the more flexible torsional angles (as the inter-ring or the chain dihedrals) is well reproduced and in agreement with both theoretical and experimental findings.

In conclusion, hybrid potentials turn out to be useful in modeling very large molecules, where the computational costs do not allow more complex functions. For example, the recently discover banana molecules,[58] which are formed from several phenyl groups, connected by benzoate linkages, could be a relevant test case for the capabilities of the proposed models.

Acknowledgment. The author would like to thank Prof. Ivo Cacelli for the many useful discussions and his careful reading of the manuscript. The University of Pisa is gratefully acknowledged for financial support.

Note Added after ASAP Publication. This article was released ASAP on March 28, 2006, with the incorrect Received Date. The correct version was posted on April 12, 2006.

References

(1) Advances in the Computer Simulations of Liquid Crystals. *NATO ASI series;* Pasini, P., Zannoni, C., Eds.; Kluwer: Dordrecht, 2000.

(2) Computer Simulations of Liquid Crystals and Polymers. *NATO ASI series;* Pasini, P., Zannoni, C., Zumer, S., Eds.; Kluwer: Dordrecht, 2005.

(3) Zannoni, C. *J. Mater. Chem.* **2001**, *11*, 2637.

(4) Crain, J.; Komolkin, A. *Adv. Chem. Phys.* **1999**, *109*, 39.

(5) Wilson, M. *Int. Rev. Phys. Chem.* **2005**, *24*, 421.

(6) Lebwohl, P.; Lasher, G. *Phys. Rev. A* **1972**, *6*, 426.

(7) M. P. Allen, G. T. Evans, D. F.; Mulder, B. *Adv. Chem. Phys.* **1993**, *86*, 1.

(8) Zewdie, H. *J. Chem. Phys.* **1998**, *108*, 2117.

(9) Gay, J. G.; Berne, B. *J. Chem. Phys.* **1981**, *74*, 3316.

(10) Cleaver, D. J.; Care, C. M.; Allen, M. P.; Neal, N. P. *Phys. Rev. E* **1996**, *54*, 559.

(11) Bates, M.; Luckhurst, G. *Struct. Bonding (Berlin)* **1999**, *94*, 65.

(12) Cross, C. W.; Fung, B. M. *J. Chem. Phys.* **1994**, *101*, 6839.

(13) LaPenna, G.; Catalano, D.; Veracini, C. A. *J. Chem. Phys.* **1996**, *105*, 7097.

(14) Wilson, M. *J. Chem. Phys.* **1997**, *107*, 8654.

(15) McBride, C.; Wilson, M. R. *Mol. Phys.* **1999**, *97*, 511.

(16) Cacelli, I.; Campanile, S.; Prampolini, G.; Tani, A. *J. Chem. Phys.* **2002**, *117*, 448.

(17) Fukunaga, H.; Takimoto, J.; Aoyagi, T.; Shoji, T.; Sawa, F.; Doi, M. *Mol. Cryst. Liq. Cryst.* **2001**, *365*, 739.

(18) Cacelli, I.; Cinacchi, G.; Geloni, C.; Prampolini, G.; Tani, A. *Mol. Cryst. Liq. Cryst.* **2003**, *395*, 171.

(19) Cacelli, I.; Cinacchi, G.; Prampolini, G.; Tani, A. *Computer Simulation of Mesogen with ab initio Interaction Potentials in Novel Approaches to the Structure and Dynamics of Liquids. Experiments, Theories and Simulation;* Samios, J., Durov, V., Eds.; Kluwer: Dordrecht, 2004.

(20) Fukunaga, H.; Takimoto, J.; Doi, M. *J. Chem. Phys.* **2004**, *120*, 7800.

(21) Lyunin, A.; Barwani, M.; Allen, M.; Wilson, M.; Neelov, I.; Allsopp, N. *Macromolecules* **1998**, *31*, 4626.

(22) Wilson, M.; Stimson, L.; Ilnytsky, J.; Hughes, Z. *Computer simulation of liquid crystalline polymers and dendrimers in Computer Simulations of Liquid Crystals and Polymers NATO ASI series;* Pasini, P., Zannoni, C., Zumer, S., Eds.; Kluwer: Dordrecht, 2005.

(23) Jorgensen, W. *BOSS 4.2;* Department of Chemistry: Yale, 2001.

(24) Amovilli, C.; Cacelli, I.; Campanile, S.; Prampolini, G. *J. Chem. Phys.* **2002**, *117*, 3003.

(25) Bizzarri, M.; Cacelli, I.; Prampolini, G.; Tani, A. *J. Phys. Chem. A* **2004**, *108*, 10336.

(26) Cacelli, I.; Prampolini, G.; Tani, A. *J. Phys. Chem. B* **2005**, *109*, 3531.

(27) Kovacic, P.; Jones, M. *Chem. Rev.* **1987**, *87*, 357.

(28) Cacelli, I.; Prampolini, G. *J. Phys. Chem. A* **2003**, *107*, 8665.

(29) Picken, S. J.; VanGunsteren, W. F.; VanDujen, P. T.; DeJeu, W. H. *Liq. Cryst.* **1989**, *6*, 357.

(30) Komolkin, A. V.; Laaksonen, A.; Maliniak, A. *J. Chem. Phys.* **1994**, *101*, 4103.

(31) Stevensson, B.; Komolkin, A.; Sandström, D.; Maliniak, A. *J. Chem. Phys.* **2001**, *114*, 2332.

(32) Zakharov, A.; Komolkin, A. V.; Maliniak, A. *Phys. Rev. E* **1999**, *59*, 6802.

(33) Zakharov, A.; Maliniak, A. *Eur. Phys. J. E* **2001**, *4*, 435.

(34) DeGaetani, L.; Prampolini, G.; Tani, A. *J. Phys. Chem. B* **2006**, *110*, 2847.

(35) Buckingam, A. *Adv. Chem. Phys.* **1978**, *12*, 107.

(36) Wiener, S. J.; Kollmann, P. A.; Nguyen, D. T.; Case, D. A. *J. Comput. Chem.* **1986**, *7*, 230.

(37) Metropolis, N.; Rosenbluth, A. W.; Rosenbluth, M. H.; Teller, A. H.; Teller, E. *J. Chem. Phys.* **1953**, *21*, 1087.

(38) Allen, M.; Tildesley, D. *Computer Simulation of Liquids;* Clarendon: Oxford, 1987.

(39) Ewald, P. P. *Ann. Phys.* **1921**, *64*, 253.

(40) *The Molecular Dynamics of Liquid Crystals NATO ASI series;* Luckhurst, G. R., Veracini, C. A., Eds.; Kluwer: Dordrecht, 1994.

(41) Bates, M.; Luckhurst, G. *J. Chem. Phys.* **1999**, *110*, 7087.

(42) Cacelli, I.; Cinacchi, G.; Prampolini, G.; Tani, A. *J. Am. Chem. Soc.* **2004**, *126*, 14278.

(43) Cacelli, I.; Cinacchi, G.; Prampolini, G.; Tani, A. *J. Chem. Phys.* **2004**, *120*, 3648.

(44) Tsuzuki, S.; Tanabe, K. *J. Phys. Chem.* **1991**, *95*, 139.

(45) Goller, A.; Grummt, U. *Chem. Phys. Lett.* **2000**, *321*, 399.

(46) Tsusuki, S.; Uchimaru, T.; Matsamura, K.; M., M. M.; Tanabe, K. *J. Chem. Phys.* **1999**, *110*, 2858.

(47) Smit, G. *Mol. Cryst. Liq. Cryst.* **1977**, *49*, 207.

(48) Irvine, P. A.; Wu, C.; Flory, P. *J. Chem. Soc., Faraday Trans.* **1984**, *80*, 1795.

(49) Dingrmans, T.; Murthy, N.; Samulski, E. *J. Phys. Chem. B* **2001**, *105*, 8845.

(50) Bastiansen, O.; Fernholt, L.; Cyvin, B. C. S.; Samdal, S.; Almenningen, A. *J. Mol. Struct.* **1985**, *128*, 59.

(51) Bastiansen, O.; Samdal, S. *J. Mol. Struct.* **1985**, *128*, 115.

(52) Steele, D.; Eaton, V. *J. Chem. Soc., Faraday Trans.* **1973**, *69*, 1601.

(53) Delugeard, Y.; Charbonneau, G. *Acta Crystallogr. B* **1976**, *33*, 1586.

(54) Baker, K.; Fratini, A.; Resch, T.; Knachel, H.; Adams, W.; Socci, E.; Farmer, B. *Polym. Pap.* **1993**, *69*, 1601.

(55) Sandmann, M.; Hamann, F.; Wurflinger, A. *Z. Naturforsh.* **1997**, *52*, 739.

(56) Adam, C.; Ferrarini, A.; Wilson, M.; Ackland, G.; Crain, J. *Mol. Phys.* **1999**, *97*, 541.

(57) Oweimreen, G.; Morsy, M. *Thermochim. Acta* **2000**, *346*, 37.

(58) Pelzl, G.; Diele, S.; Weissflog, W. *Adv. Mater.* **1999**, *11*, 707.

CT050328O